Visible Light Mediated Bidirectional Control over Carbonic Anhydrase Activity in Cells and *in Vivo* Using Azobenzenesulfonamides

Kanchan Aggarwal,

Department of Chemistry, University of Texas at Austin, Austin, Texas 78712, United States

Timothy P. Kuka,

Department of Molecular Biosciences and Institute for Cellular and Molecular Biology, University of Texas at Austin, Austin, Texas 78712, United States

Mandira Banik,

Department of Chemistry, University of Texas at Austin, Austin, Texas 78712, United States

Brenda P. Medellin,

Department of Molecular Biosciences and Institute for Cellular and Molecular Biology, University of Texas at Austin, Austin, Texas 78712, United States

Chinh Q. Ngo,

Department of Chemistry, University of Texas at Austin, Austin, Texas 78712, United States

Da Xie,

Department of Chemistry, University of Texas at Austin, Austin, Texas 78712, United States

Yohaan Fernandes,

Department of Molecular Biosciences and Institute for Cellular and Molecular Biology, University of Texas at Austin, Austin, Texas 78712, United States; Waggoner Center for Alcohol and Addiction Research, The University of Texas at Austin, Austin, Texas 78712, United States

Tyler L. Dangerfield,

Department of Molecular Biosciences and Institute for Cellular and Molecular Biology, University of Texas at Austin, Austin, Texas 78712, United States

Elva Ye,

Department of Chemistry, University of Texas at Austin, Austin, Texas 78712, United States

Corresponding Author emilyque@cm.utexas.edu.

ASSOCIATED CONTENT

Supporting Information and (cif) The Supporting Information is available free of charge at https://pubs.acs.org/doi/10.1021/jacs.0c05383.

General materials and synthetic methods, experimental protocols, tables and figures, sample characterization data, and supporting explanation of TD-DFT calculation (PDF)

Crystal data of *t*-CAP-F5 (CIF)

Crystal data of *c*-CAP-F5 (CIF)

Complete contact information is available at: https://pubs.acs.org/10.1021/jacs.0c05383

Notes

The authors declare no competing financial interest.

Bailey Bouley,

Department of Chemistry, University of Texas at Austin, Austin, Texas 78712, United States

Kenneth A. Johnson,

Department of Molecular Biosciences and Institute for Cellular and Molecular Biology, University of Texas at Austin, Austin, Texas 78712, United States

Yan Jessie Zhang,

Department of Molecular Biosciences and Institute for Cellular and Molecular Biology, University of Texas at Austin, Austin, Texas 78712, United States

**Johann K. Eberhart**,

Department of Molecular Biosciences and Institute for Cellular and Molecular Biology, University of Texas at Austin, Austin, Texas 78712, United States; Waggoner Center for Alcohol and Addiction Research, The University of Texas at Austin, Austin, Texas 78712, United States

Emily L. Que

Department of Chemistry, University of Texas at Austin, Austin, Texas 78712, United States

Abstract

Two azobenzenesulfonamide molecules with thermally stable *cis* configurations resulting from fluorination of positions *ortho* to the azo group are reported that can differentially regulate the activity of carbonic anhydrase in the *trans* and *cis* configurations. These fluorinated probes each use two distinct visible wavelengths (520 and 410 or 460 nm) for isomerization with high photoconversion efficiency. Correspondingly, the *cis* isomer of these systems is highly stable and persistent (as evidenced by structural studies in solid and solution state), permitting regulation of metalloenzyme activity without continuous irradiation. Herein, we use these probes to demonstrate the visible light mediated bidirectional control over the activity of zinc-dependent carbonic anhydrase in solution as an isolated protein, in intact live cells and *in vivo* in zebrafish during embryo development.

Graphical abstract
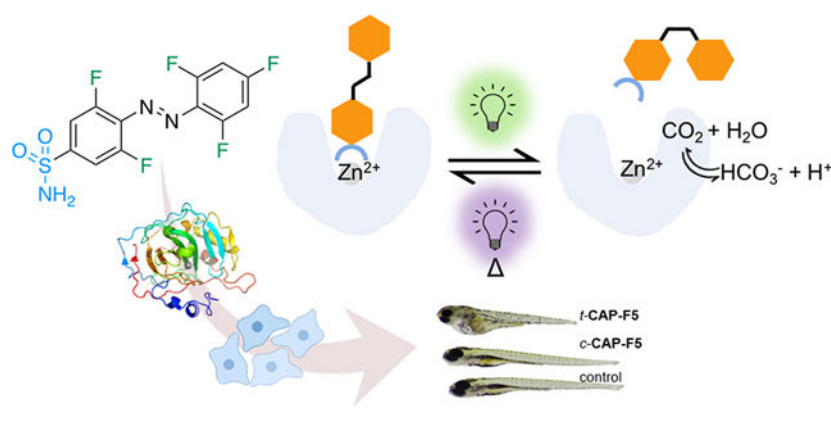
INTRODUCTION

Photopharmacology, in which the activity of pharmacophores can be controlled via application of specific wavelengths of light, has emerged as an attractive method for controlling the behavior of biological species on demand. Light serves as an ideal external control element for *in situ* biochemical manipulation because it offers a high level of spatiotemporal resolution, it is minimally invasive, and its wavelength and intensity can be readily tuned. One important strategy used in the development of photoactivatable probes is alteration of the properties of a molecule (chemical structure, shape, polarity) upon light irradiation, resulting in different affinity toward the desired target. Recent years have seen great advances in this field where the control over biomacromolecular function has been attained either by using a photoprotecting group[1] (irreversible approach) or small photochromic moieties[2] (reversible approach). The latter approach uses a photoswitchable bond that allows access to different molecular structures induced by irradiation of light. Although stilbenes, hemithioindigos, and diarylethenes have been used as switches, azobenzenes show the most promise in achieving a larger range of activation wavelengths and greater photoactivated state stabilities.[3] They have been readily used to manipulate a wide variety of biological processes,[4] including regulation of protein expression,[5] enzyme folding,[6] and activity[7,8] and DNA conformation and transcription[9,10] and have been explored in the fields of chemotherapeutics[11,12] and neurobiology.[13,14]

Carbonic anhydrase (CA) is a promising target for photoregulation due to its physiological and pathological roles.[15] The active site of most CAs contains a zinc ion bound to three histidine residues and one water molecule. This protein catalyzes a simple physiological reaction, the reversible conversion of carbon dioxide and water to bicarbonate and protons. CAs are involved in the maintenance of acid-base equilibrium and CO2 homeostasis. However, they can be highly overexpressed in diseases, including cancer, epilepsy, and glaucoma, and hence are important therapeutic targets.[16] Effective photoswitchable inhibitors of CA have promise as research tools as they can be activated in a spatially and temporally specific manner. Therapeutic applications are also possible, particularly for glaucoma due to its location in the eye where light activation is very feasible.[17]

Aryl sulfonamides show exquisite selectivity for CA inhibition, combining metal coordination, hydrogen bonding, and hydrophobic interactions to achieve this specificity.[18] Others have reported azobenzene-based photoswitches for CA; however, studies have been limited to isolated protein or cell lysates.[19–21] Recently, we reported small molecule azobenzenesulfonamide CAP1 that demonstrated differential regulation of intracellular pH in the *trans* and *cis* isomeric forms in live cancer cells.[22] However, this probe had three major limitations: use of UV light for photoisomerization, poor photoconversion efficiency, and importantly, poor thermal stability of the *cis* isomer, which limited long-term applications in live cells and organisms.

To address these limitations, we identified *ortho*-fluorination as a strategy to improve the performance of azobenzene-based probes. Fluorination *ortho* to the azo moiety of the azobenzene results in separation of the n-π^* absorption band in the *trans* and *cis* isomers.[23] This splitting of absorption bands can further be increased by the incorporation of an

electron withdrawing group at the position *para* to the azo unit. This large separation of n-π^* bands enables use of distinct visible wavelengths to achieve higher isomer conversion in the photostationary state when compared to other azobenzene derivatives. Remarkably, the *cis* isomers of *ortho*-fluorinated azobenzenes are exceptionally thermally stable with half-lives as long as several days.[24] Furthermore, unlike other visible light sensitive and stable *cis*-azobenzene derivatives, *ortho*-fluorinated systems are immune to the cytosolic reducing environment, making them more biocompatible.[25] *Ortho*-fluorinated azobenzenes have been extensively used for materials applications[13,26–29] and have gained interest recently in biological applications,[30–34] demonstrating the robustness of this system in the context of biomolecules and cells. Herein, we report the first demonstration of the *ortho*-fluorination strategy for controlling the activity of a metalloenzyme. Importantly, we demonstrate the efficacy of this approach for dynamic modulation of the activity of Zn-dependent carbonic anhydrase *in vitro* with isolated protein, in live cells and, for the first time, *in vivo* in live zebrafish.

RESULTS AND DISCUSSION

We synthesized and characterized two fluorinated azobenzenesulfonamide probes containing either three (CAP-F3) or five (CAP-F5) fluorines. We anticipated that these probes would achieve red-shifted wavelengths of isomerization relative to nonfluorinated derivatives with improved switching fidelities and increased thermal lifetime of the *cis* isomer (Scheme 1). Full experimental details are provided in the Supporting Information.

The photoisomerization properties of CAP-F3 and CAP-F5 were monitored in methanol (Figure 1A and 1B) and aqueous buffer (Figure S1) using UV-vis absorption spectroscopy. All relevant wavelengths are summarized in Table S1. The spectra display absorption bands corresponding to a π-π^* transition (S_2) with a λ_{max} of 312 nm for CAP-F3 and 306 nm for CAPF5. Furthermore, moderate absorbance bands at 436 nm for CAP-F3 and 450 nm for CAP-F5 were observed, which correspond to n-π^* transitions (S_1). Irradiation of CAP-F3 and CAP-F5 with 520 nm light shifted their absorption profiles to ones consistent with *cis* isomer formation, including a significant decrease in the intensity of the π-π^* band. While the π-π^* bands underwent a slight hypsochromic shift in both cases, there was a large hypsochromic shift in the n-π^* transition by 16 nm for CAP-F3 and 37 nm for CAP-F5 upon photoisomerization (Table S1). The large separation of the n-π^* transition bands between *trans* and *cis* isomers should result in high photoisomerization conversions.[23] Indeed, irradiation of solutions with 520 nm light yielded high conversions to *c*-CAP-F3 (71%) and *c*-CAP-F5 (87%) (^{19}F NMR, CD_3OD, Figure S3). Isomerization from *cis* to *trans* can subsequently be achieved by irradiating with 460 and 410 nm light for CAP-F3 (58%) and CAP-F5 (82%) respectively. The high conversion of CAP-F5 in aqueous buffer is better than our previously reported probes (CAP1 and CAP2),[22] and is on the same order as other *cis*-*trans* isomerizing photoswitches studied in buffer solution.[2]

To further understand the spectroscopic properties, we performed time-dependent density functional theory (TDDFT) calculations to compute the energies of the HOMO (n) and LUMO (π^*) orbitals for both the *trans* and *cis* isomers of CAP-F3 and CAP-F5 at the B3LYP/6–31G* level and also included calculations for a CAP-F1 analogue, where the

ortho-fluorine atoms are all substituted by hydrogen atoms. The n and π^* orbitals of the *cis* isomers are all higher in energy than the *trans* isomers. However, the relative energy of the n orbital is also affected by the number of *ortho*-fluorine atoms due to the σ-electron withdrawing effect of fluorine. As a result, the calculations predicted a larger separation of n-π^* transition bands between the *trans* and *cis* isomers for CAP-F5 compared to CAP-F3 or CAP-F1 analogues (Table S1), demonstrating the importance of *ortho*-fluorination in our molecular design. A detailed explanation of calculations and interpretation is provided in the Supporting Information.

The *cis* isomers of CAP-F3 and CAP-F5 both have increased thermal stability compared to nonfluorinated analogues,[22] with exceptional thermal stability exhibited for c-CAP-F5. The thermal conversion from the *cis* to *trans* isomer of CAP-F3 and CAP-F5 at 37 °C in aqueous buffer was studied under dark conditions (Figure 2A). We observed a low ~15% conversion of *c*-CAP-F5 to *t*-CAP-F5 over 48 h, and a ~40% conversion of *c*-CAP-F3 to *t*-CAP-F3. This difference is unsurprising given the n-π^* separation trend. The stability driven by *ortho*-fluorination is better than what has been observed for *ortho*-methyl substituted bistable azobenzenes.[35] Previous reports have indicated that intramolecular interactions may also contribute to the stability of the *cis* isomer of *ortho*-fluorinated derivatives of azobenzene.[36,37]

We examined potential interactions using NMR spectroscopy in a polar protic solvent. In the ^{19}F NMR spectrum of CAP-F5, we observed that the peak splitting pattern for the *cis* isomer was more complex than the *trans* isomer (Figure 2B) and could not be accounted for solely by through-bond couplings. The decoupled [19]F-{[1]H} spectrum was collected and revealed coupling between F_a and F_b only in the *cis* isomer.[37] As shown in Figure 2B, the peaks corresponding to F_a and F_b in the *trans* isomer appeared as singlet and doublet (due to the *para*-F), respectively, and hence, there was no evidence of through-space coupling between the *ortho*-fluorine moieties in this isomeric form. The peaks corresponding to F_a and F_b in the *cis* isomer appear as a triplet and quartet, respectively, as a result of through-space coupling between the *ortho*-fluorines ($^{TS}J_{FF}$ = 5.64 Hz for F_a, 5.67 Hz for F_b).[38] Coupling between F_a and F_b in the *cis* isomer was further supported by correlation peaks observed in its ^{19}F–^{19}F COSY spectrum (Figure S9). Finally, we investigated how the rotation of the ring bearing F_b is affected by the absence (CAP-F3) or presence (CAP-F5) of F_a on the other phenyl ring using *trans*verse relaxation time (T_2) measurements.[39] The shorter T_2 values of F_b in the *cis* isomer (1.19 s for cCAP-F3; 0.73 s for c-CAP-F5) indicate that ring rotation is more constrained in *c*-CAP-F5; this constriction likely stabilizes *c*-CAP-F5 in solution greater than *c*-CAP-F3.

The persistence of *c*-CAP-F5 was further demonstrated in the solid state via single-crystal X-ray diffraction, a rare example of a *cis*-azobenzene structure.[36] In the crystal structure, the distances between the *ortho*-fluorine atoms and ipso carbons are 2.78 and 2.76 Å (Figure 2C). Both distances are shorter than the C-F van der Waals distance (3.17 Å), demonstrating the presence of C···F interactions in the *cis* isomer. Such favorable interactions were not observed in the solid-state structure of *t*-CAP-F5 (Figure 2D). The increased stabilization of these C···F interactions should result in a smaller Gibbs free energy difference between the

trans and *cis* isomers, and DFT calculated energies reflected this when CAP-F5, CAP-F3, and CAP-F1 were compared ($\Delta G_{cis\text{-}trans}$, Table S2).[36]

Due to the increased thermal stability and higher photoisomerization efficiency of *c*-CAP-F5 over *c*-CAP-F3, we focused on CAP-F5 for more in-depth studies. The binding interactions of *t*-CAP-F5 and *c*-CAP-F5 were studied with bovine carbonic anhydrase (bCA) using a dansylamide (DNSA) competition assay. DNSA, a sulfonamide based CA-inhibitor, exhibits an enhanced fluorescence at 458 nm upon binding to the active site of CA (apparent K_d = 1.6 μM, under our experimental conditions, Figure S10A), and a weakened fluorescence when an external ligand displaces it from the active site (Figure S11). A solution of bCA·DNSA was titrated with *trans* and *cis* isomers of CAP-F5, and the apparent K_d values were calculated. As shown in Figure 3A, the binding profiles of the *trans* and *cis* isomers are drastically different, yielding K_d' values of 9 ± 1.3 nM for *t*-CAP-F5 and 106 ± 16 nM for *c*-CAP-F5, demonstrating an order higher binding affinity of the *trans* isomer.

A control molecule lacking the Zn^{2+}-binding *p*-sulfonamide group (CAP-con, Scheme S3) induces almost no change in the fluorescence emission (Figure S12). We further employed DNSA to investigate the isomerization of CAP-F5 in the active site of CA, using CAP-F5, bCA, and an excess of DNSA. Solutions of bCA, DNSA, and CAP-F5 were irradiated with 520 nm (*trans* → *cis*) and 410 nm (*cis* → *trans*) alternately with fluorescence measured after each irradiation (Figure 3B). DNSA fluorescence intensity decreased after irradiation with 410 nm and increased after irradiation with 520 nm through several cycles. These experiments demonstrate the reversible and robust CAP-F5 photoisomerization the binding profiles of the trans and cis isomers are drastically different, yielding K_d' values of 9 ± 1.3 nM for *t*-CAP-F5 and 106 ± 16 nM for *c*-CAP-F5, demonstrating an order higher binding affinity of the *trans* isomer.

A control molecule lacking the Zn^{2+}-binding *p*-sulfonamide group (CAP-con, Scheme S3) induces almost no change in the fluorescence emission (Figure S12). We further employed DNSA to investigate the isomerization of CAP-F5 in the active site of CA, using CAP-F5, bCA, and an excess of DNSA. Solutions of bCA, DNSA, and CAP-F5 were irradiated with 520 nm (*trans* → *cis*) and 410 nm (*cis* → *trans*) alternately with fluorescence measured after each irradiation (Figure 3B). DNSA fluorescence intensity decreased after irradiation with 410 nm and increased after irradiation with 520 nm through several cycles. These experiments demonstrate the reversible and robust CAP-F5 photoisomerization even in the presence of CA.

To better understand the difference in binding preference between the *cis* and *trans* isomers of CAP-F5 toward CA, we analyzed the X-ray structure of hCAII with a related a z o b e n z e n e s u l f o n a m i d e l i g a n d , (*E*) - 4 - (4 aminophenyldiazenyl)benzenesulfonamide (L), bound to the active site (Protein Data Bank: 5BYI).[40] In this crystal structure, L forms extensive hydrophilic and hydrophobic interactions with hCAII at the Zn active site (Figure 4A). The primary interaction between the protein and L is between the deprotonated nitrogen of the $-SO_2NH_2$ and the Zn^{2+} center, forming a tetrahedral coordination along with the three active site histidines (H94, 96, and 119). The sulfonamide group of L also hydrogen bonds to the backbone and side chain of Thr198, while the adjoining benzene ring

sits in a hydrophobic pocket formed by residues W208, L197 and L142. The other phenyl ring hydrophobically stacks with P201 and forms a 6 Å T-shape $\pi-\pi$ stacking with F130 (Figure 4A).

The molecular structure of CAP-F5 highly resembles that of L with the only alteration at the benzyl ring extending away from the Zn^{2+} coordination site. We conducted molecular modeling and docking using Maestro (Schrodinger Suite).[41] Due to the high structural similarity of t-CAP-F5 to L, the same coordination to Zn^{2+} is expected to be conserved. The model is then energy minimized in Maestro.[42,43] Two configurations of t-CAP-F5 are identified with favorable energy, both maintaining similar binding mode to L without any steric clashes (Figure 4A, B). The first configuration is identical to the crystal structure of L binding with all favorable interaction maintained (Figure 4A). The addition of fluorine atoms in CAP-F5, however, decreases the electron-richness of the benzene rings compared to L. Thus, an additional binding mode is also possible for t-CAP-F5 when the azo bond flips by 180° (Figure 4B). In this alternative configuration with similar favorable binding energy, the fluoro-benzene ring rotates to a configuration that forms a parallel $\pi-\pi$ stacking of 3.7 Å with F130 while maintaining almost all other noncovalent interactions. This orientation can be further stabilized by a potential hydrogen bond between the azo group and Q92 with no steric clashes with residues forming the active site pocket (Figure 4B). Thus, t-CAP-F5 forms extensive favorable contacts with the enzyme in two possible poses.

When docking c-CAP-F5, the favorable interaction between the Zn^{2+} and the sulfonamide nitrogen of the ligand cannot be retained (Figure 4C). In order to maintain the same coordination to Zn^{2+}, the distal phenyl ring would be in close contact with the active site pocket due to the cis-configuration of the azo group, causing clashes with Q92, V121, V142, and H64 (Figure 4C). To avoid steric clashes, c-CAP-F5 has to adapt to a configuration retreating from the deep active site pocket containing the Zn^{2+}. As a result, the distance between the sulfonamide nitrogen and the Zn^{2+} increase from 2.0 Å (as found in L and more likely in tCAP-F5) to 3.6 Å, which is no longer optimal for Zn^{2+} coordination (Figure 4D). Furthermore, the hydrogen bond between T198 and the sulfonamide group's nitrogen in the azobenzene ligand is unlikely to form in this configuration (Figure 4D). Thus, c-CAP-F5 cannot show any favorable interaction with Zn^{2+} in the active site, which makes it more weakly binding than t-CAP-F5.

CA catalyzes the hydration of CO_2 and dehydration of HCO_3^- reversibly. The inhibitory effect of the $trans$ and cis isomers of CAP-F5 on CO_2 hydration activity of bCA was measured by tracking changes in solution pH using phenol red as a pH indicator, and a solution of saturated CO_2 as a substrate (Figure 5A).[44] The observed rates for CO_2 conversion by bCA in the absence and presence of known CA inhibitor acetazolamide were 0.113 and 0.027 s^{-1}, respectively. Correspondingly, the initial velocities of the catalytic reaction in the presence of $trans$ and cis isomers of CAP-F5 were found to be 0.025 and 0.082 s^{-1}, respectively, demonstrating the superior ability of the $trans$ isomer to inhibit CA enzymatic activity. Using this same stopped flow method, the apparent K_i values for t-CAP-F5 and c-CAP-F5 were calculated to be 36 ± 2 and 164 ± 8 nM, respectively (Figure 5B), indicating ~5 times greater potency of t-CAP-F5.

As CA can also catalyze bicarbonate dehydration, we also investigated CAP-F5 in the context of this reaction, where aqueous $KHCO_3$ was used as the substrate. The initial velocity of the CA-catalyzed reaction was 0.36×10^{-2} s^{-1} in the presence of t-CAP-F5 and 1.0×10^{-2} s^{-1} in the presence of c-CAP-F5, similar to the reaction rates in the presence $(0.10 \times 10^{-2}$ $s^{-1})$ and absence of acetazolamide $(1.3 \times 10^{-2}$ $s^{-1})$ (Figure 5C). The apparent K_i values of t-CAP-F5 and c-CAP-F5 were calculated to be 30 ± 3 and 205 ± 14 nM respectively (Figure 5D). These studies show that CAP-F5 isomers can be used to modulate both the CO_2 hydration and bicarbonate dehydration activity of CA.

Having demonstrated the efficacy of CAP-F5 to differentially interact with isolated CA protein in the *trans* and *cis* isomeric forms, we next applied our photoswitch to control the activity of CA in cell culture. We note that CAP-F5 isomerization is reversible over several cycles in cell culture media (Figure S16). CAII is the cytosolic isoform of CA responsible for maintaining intracellular pH and is known to be overexpressed in certain cancer cells.[16] It has been reported that the resting intracellular pH of cells is affected by CA inhibitors, and this change highly depends on the cell type and environment.[45–47] Previously, we showed differential effects of *trans* and *cis* isomers of CAP1 on intracellular pH; however, thermal instability of *cis* isomer prevented applications over longer time periods.[22] With our improved probe design with highly stable *cis* isomer, we compared the ability of *trans* and *cis* isomers of CAP-F5 to modulate intracellular pH in HeLa cells at both short (30 min) and long (24h) incubation times. We performed a cellular cytotoxicity assay to determine probe concentrations at which minimal toxicity would be observed for the *cis* isomer (Figure S17). We observed that cells incubated with the *cis* isomer maintained a similar pH to control cells after both short and long incubation times, whereas cells incubated with the *trans* isomer displayed decreased intracellular pH in both scenarios (Figures 6A and S20). We repeated these experiments with isolated *cis* and *trans* species (via preparative HPLC), and similar results were obtained, indicating the PSS isomers are sufficient to obtain differential cellular response (Figure S20).

We next explored the effect of the isomers of CAP-F5 on the response of the cytoplasmic CA machinery to exogenous perturbations of CO_2. When the level of extracellular CO_2 increases, it passively diffuses into the cytoplasm through the cell membrane where it is converted to carbonic acid by cytoplasmic CAs, resulting in a decrease in intracellular pH (Figure 6D).[48] Inhibition of cytoplasmic CA reduces the rate of intracellular acidification following increases in extracellular CO_2 concentration.[45,46,48,49] We used this rate of change of intracellular pH to demonstrate the real-time inhibition of cytosolic CA by t-CAP-F5. In our experiment, HeLa cells were loaded with pHrodo and incubated with 25 μM t-CAP-F5, c-CAP-F5, or a DMSO control for 30 min. A bolus of saturated aqueous CO_2 was added to the cell suspension and intracellular pH changes were monitored using flow cytometry. As shown in Figure 6B, c-CAP-F5 treated cells had similar kinetic changes in intracellular pH over time as compared to DMSO-treated control cells, signifying that cytosolic CA remains active in both groups. However, t-CAPF5 treated cells displayed a slower rate of change in pH upon CO_2 addition, consistent with inhibition of the cytosolic CA machinery of CO_2 hydration (Figure 6C).

Intracellular c-CAP-F5 can further be photostimulated *in situ* to activate CA inhibition. Cells were treated with pHrodo dye, c-CAP-F5, or DMSO in the similar way as described earlier. The c-CAP-F5 treated cells were divided into two groups, where only one group was irradiated with 410 nm light for 3 min (no phototoxicity observed) to isomerize the *cis* form to *trans* form *in situ* right before the addition of CO_2, and were compared with nonirradiated cells. As shown in Figure 6E, the kinetics of intracellular pH change in *cis* treated cells was faster than cells irradiated with 410 nm (converting *cis* to *trans*) prior to the addition of CO_2. This experiment demonstrates that probe isomerization can be achieved within the complex cellular environment, and indeed could be used to inhibit the CA activity upon light irradiation.

Next, we applied CAP-F5 in an *in vivo* system. Embryonic zebrafish (*Danio rerio*) are an excellent animal model for studying drug induced toxicity due to their high fecundity, external fertilization, rapid development, and the ease of maintaining large numbers in a small space.[50] Substances of interest can be administered in the media and then are rapidly up taken into the embryo. Importantly, the embryos are also optically transparent, which allows for study of photo-responsive materials. CA is a vital component in acid-base regulation as well as ionic and osmotic balance in vertebrates.[51] Just like mammals, fish possess an abundance of CA isoforms that vary in molecular sequence, tissue distribution, and subcellular localization.[52] They also have different kinetic properties and active site structure and thus different susceptibility to inhibitors. They are necessary during the early stages of development in zebrafish for effective CO_2 excretion.[53] Inhibition of CA by inhibitors like acetazolamide has a great effect on zebrafish embryogenesis; embryos treated with CA inhibitor can display small otoliths, an irregular jaw, enlarged heart and yolk sac, and impaired locomotion.[54,55]

We used phenotypic analysis to differentiate the behavior of *cis* and *trans* CAP-F5 in zebrafish. Wild-type (AB strain) embryos were collected and transferred into standard embryo media[56] and sorted by developmental stage.[57] At 6 h post fertilization (6 hpf), zebrafish were exposed to media containing 1% DMSO and varying concentrations of CAPF5 in both *trans* and *cis* forms. Embryos were incubated in a light-proof container at 28.5 °C until 48 hpf. They were then transferred to fresh media and raised to 5 days post fertilization (5dpf), when they were assessed for viability (Figure 7A). As expected, t-CAP-F5 induces higher toxicity than c-CAP-F5 (Table S5). Further, the distinct effect of the isomers on embryogenesis was evaluated. For morphological end points, the zebrafish were treated with 2.5 μM of *trans* and *cis* isomers of CAP-F5 and were raised to 5dpf as described above. As shown in Figure 7B, zebrafish treated with t-CAP-F5 showed multiple morphological abnormalities, including failure to form a swim bladder, pectoral fin defects, and cardiac edema, consistent with previous reported effects of CA inhibitors.[54,55] One-hundred percent of embryos ($n = 30$) treated with the same concentration of c-CAP-F5 developed normally, signifying the normal function of CA in *cis*-treated fish. Furthermore, the zebrafish were fixed and processed for otolith analysis. The t-CAP-F5 treated zebrafish had hollow and underdeveloped otoliths as opposed to c-CAP-F5 treated fish, where 100% ($n = 30$) had normally developed otoliths (Figure 7D). This is likely caused by the inhibition of CA isoforms present in inner ear hair cells by t-CAP-F5 only, disrupting the supply of HCO_3^- to the endolymph for otolith calcification.[56] Potentially as a result of poor otolith

development or other developmental defects, fish treated with *t*-CAP-F5 showed poor locomotion, while *c*-CAP-F5 treated fish exhibited normal locomotive behavior (Figure 7C). Our results signify that the isomers of CAP-F5 are capable of differential effects in this complex multicellular system that are associated with CA inhibition.

After establishing that different isomers of CAP-F5 can have different effects on the developmental and behavioral properties of fish, we investigated if the probe could be activated in situ within the embryo for CA inhibition during development. Embryos were treated with *c*-CAP-F5 as described above, but the probe was activated to the *trans* isomer *in situ* (within the fish) through photoirradiation with 410 nm (0.50 mW/cm^2; 3 min) at different time points during embryogenesis (12, 24, 30 hpf), delineated in Figure 7A. These irradiation conditions do not affect the development of embryos at any given irradiation time point. As CA isoforms play an important role in meeting the requirements for CO_2 excretion between 24 and 48 hpf in developing fish, these time points were chosen to assess the effect of inhibition before and during that window.[53] The results were compared to fish that were treated with *ex situ* generated *trans* isomer (positive control) and vehicle (negative control) at all the respective time of *cis* activation. The degree of edema observed in the photoactivated fish are similar to the *t*-CAPF5 treated fish at all points of photoirradiation, signifying the capability of activating the probe within the embryos (Figure 7E). Moreover, as we progress further along the postfertilization timeline for probe activation, the inhibitor efficacy appears to be decreasing. These results are consistent with the known crucial role of CA in the initial phases of fish development.[53] Otolith development at various stages of probe activation shows a similar trend (Figure 7F), further corroborating the relation of phenotypic changes with *in situ* CA inhibition in this live organism model system. These experiments represent a key demonstration of using *cis* stabilized *ortho*-fluorinated azobenzenes in an *in vivo* system and achieving *in situ* photoactivation over extended time periods (up to 48 h).

CONCLUSIONS

In conclusion, we demonstrated the *in vitro*, cellular, and *in vivo* application of an azobenzene photopharmacophore that targets the active site of the metalloenzyme carbonic anhydrase. *Ortho*-fluorination serves to red-shift photoisomerization wavelengths, improve photoconversion efficiency, and importantly, stabilize the *cis* isomer. These properties enable longitudinal studies in cells and, for the first time, *in vivo*, allowing *in situ* temporal control of CA activity and demonstrating the potential use of this strategy for spatially and temporally regulated metalloenzyme activity. These strategies should not be limited to carbonic anhydrase, and current efforts are focused on targeting metalloenzyme classes with relevance to cancer and other diseases.

Supplementary Material

Refer to Web version on PubMed Central for supplementary material.

ACKNOWLEDGMENTS

ABBREVIATIONS

|	
CAP1	carbonic anhydrase azobenzene photoswitch 1
CAP2	carbonic anhydrase azobenzene photoswitch 2
CAP-F3	carbonic anhydrase azobenzene photoswitch with three fluorines
CAP-F5	carbonic anhydrase azobenzene photoswitch with five fluorines
CAP-con	carbonic anhydrase azobenzene photoswitch control with no sulfonamide
CA	carbonic anhydrase
DFT	density functional theory
DNSA	dansylamide
t	solution after irradiation with 410 nm (CAPF5) or 460 nm (CAP-F3) light
c	solution after irradiation with 520 nm light
PSS	photostationary state
NMR	nuclear magnetic resonance
XRD	X-ray diffraction
$^{TS}J_{FF}$	through space coupling constant between fluorine atoms

REFERENCES

(1). Klan P; Solomek T; Bochet CG; Blanc A; Givens R; Rubina M; Popik V; Kostikov A; Wirz J Photoremovable protecting groups in chemistry and biology: reaction mechanisms and efficacy. Chem. Rev 2013, 113 (1), 119–91. [PubMed: 23256727]

(2). Szymanski W; Beierle JM; Kistemaker HA; Velema WA; Feringa BL Reversible photocontrol of biological systems by the incorporation of molecular photoswitches. Chem. Rev 2013, 113 (8), 6114–78. [PubMed: 23614556]

(3). Mahimwalla Z; Yager KG; Mamiya J; Shishido A; Priimagi A; Barrett CJ Azobenzene photomechanics: prospects and potential applications. Polym. Bull 2012, 69 (8), 967–1006.

(4). Beharry AA; Woolley GA Azobenzene photoswitches for biomolecules. Chem. Soc. Rev 2011, 40 (8), 4422–37. [PubMed: 21483974]

(5). Ogasawara S Duration Control of Protein Expression in Vivo by Light-Mediated Reversible Activation of Translation. ACS Chem. Biol 2017, 12 (2), 351–356. [PubMed: 28049292]

(6). Martin N; Ruchmann J; Tribet C Prevention of aggregation and renaturation of carbonic anhydrase via weak association with octadecyl- or azobenzene-modified poly(acrylate) derivatives. Langmuir 2015, 31 (1), 338–49. [PubMed: 25495869]

(7). Weston CE; Kramer A; Colin F; Yildiz O; Baud MG; Meyer-Almes FJ; Fuchter MJ Toward Photopharmacological Antimicrobial Chemotherapy Using Photoswitchable Amidohydrolase Inhibitors. ACS Infect. Dis 2017, 3 (2), 152–161. [PubMed: 27756124]

(8). Szymanski W; Ourailidou ME; Velema WA; Dekker FJ; Feringa BL Light-Controlled Histone Deacetylase (HDAC) Inhibitors: Towards Photopharmacological Chemotherapy. Chem. Eur. J 2015, 21 (46), 16517–24. [PubMed: 26418117]

(9). Wang X; Huang J; Zhou Y; Yan S; Weng X; Wu X; Deng M; Zhou X Conformational switching of G-quadruplex DNA by photoregulation. Angew. Chem., Int. Ed 2010, 49 (31), 5305–09.

(10). Tian T; Song Y; Wang J; Fu B; He Z; Xu X; Li A; Zhou X; Wang S; Zhou X Small-Molecule-Triggered and Light-Controlled Reversible Regulation of Enzymatic Activity. J. Am. Chem. Soc 2016, 138 (3), 955–61. [PubMed: 26741151]

(11). Sheldon JE; Dcona MM; Lyons CE; Hackett JC; Hartman MC Photoswitchable anticancer activity via trans-cis isomerization of a combretastatin A-4 analog. Org. Biomol. Chem 2016, 14 (1), 40–49. [PubMed: 26503632]

(12). Borowiak M; Nahaboo W; Reynders M; Nekolla K; Jalinot P; Hasserodt J; Rehberg M; Delattre M; Zahler S; Vollmar A; Trauner D; Thorn-Seshold O Photoswitchable Inhibitors of Microtubule Dynamics Optically Control Mitosis and Cell Death. Cell 2015, 162 (2), 403–411. [PubMed: 26165941]

(13). Tochitsky I; Banghart MR; Mourot A; Yao JZ; Gaub B; Kramer RH; Trauner D Optochemical control of genetically engineered neuronal nicotinic acetylcholine receptors. Nat. Chem 2012, 4 (2), 105–11. [PubMed: 22270644]

(14). Frank JA; Yushchenko DA; Hodson DJ; Lipstein N; Nagpal J; Rutter GA; Rhee J-S; Gottschalk A; Brose N; Schultz C; Trauner D Photoswitchable diacylglycerols enable optical control of protein kinase C. Nat. Chem. Biol 2016, 12 (9), 755–762. [PubMed: 27454932]

(15). Supuran CT Structure and function of carbonic anhydrases. Biochem. J 2016, 473 (14), 2023–32. [PubMed: 27407171]

(16). Mboge MY; Mahon BP; McKenna R; Frost SC Carbonic Anhydrases: Role in pH Control and Cancer. Metabolites 2018, 8 (1), 19.

(17). Scozzafava A; Supuran CT Glaucoma and the applications of carbonic anhydrase inhibitors. Subcell. Biochem 2014, 75, 349–59. [PubMed: 24146387]

(18). Kiefer LL; Paterno SA; Fierke CA Hydrogen Bond Network in the Metal Binding Site of Carbonic Anhydrase Enhances Zinc Affinity and Catalytic Efficiency. J. Am. Chem. Soc 1995, 117, 6831–6837.

(19). Mogaki R; Okuro K; Aida T Adhesive Photoswitch: Selective Photochemical Modulation of Enzymes under Physiological Conditions. J. Am. Chem. Soc 2017, 139 (29), 10072–10078. [PubMed: 28675032]

(20). DuBay KH; Iwan K; Osorio-Planes L; Geissler PL; Groll M; Trauner D; Broichhagen J A Predictive Approach for the Optical Control of Carbonic Anhydrase II Activity. ACS Chem. Biol 2018, 13 (3), 793–800. [PubMed: 29357237]

(21). Harvey JH; Trauner D Regulating enzymatic activity with a photoswitchable affinity label. ChemBioChem 2008, 9 (2), 191–3. [PubMed: 18085544]

(22). Aggarwal K; Banik M; Medellin B; Que EL In Situ Photoregulation of Carbonic Anhydrase Activity Using Azobenzenesulfonamides. Biochemistry 2019, 58 (1), 48–53. [PubMed: 30358990]

(23). Bleger D; Schwarz J; Brouwer AM; Hecht S o-Fluoroazobenzenes as readily synthesized photoswitches offering nearly quantitative two-way isomerization with visible light. J. Am. Chem. Soc 2012, 134 (51), 20597–600. [PubMed: 23236950]

(24). Knie C; Utecht M; Zhao F; Kulla H; Kovalenko S; Brouwer AM; Saalfrank P; Hecht S; Bleger D ortho-Fluoroazobenzenes: visible light switches with very long-Lived Z isomers. Chem. - Eur. J 2014, 20 (50), 16492–501. [PubMed: 25352421]

(25). Ahmed Z; Siiskonen A; Virkki M; Priimagi A Controlling azobenzene photoswitching through combined ortho-fluorination and -amination. Chem. Commun 2017, 53 (93), 12520–12523.

(26). Iamsaard S; Anger E; Asshoff SJ; Depauw A; Fletcher SP; Katsonis N Fluorinated Azobenzenes for Shape-Persistent Liquid Crystal Polymer Networks. Angew. Chem., Int. Ed 2016, 55 (34), 9908–12.

(27). Bushuyev OS; Tomberg A; Friscic T; Barrett CJ Shaping crystals with light: crystal-to-crystal isomerization and photomechanical effect in fluorinated azobenzenes. J. Am. Chem. Soc 2013, 135 (34), 12556–9. [PubMed: 23924402]

(28). Castellanos S; Goulet-Hanssens A; Zhao F; Dikhtiarenko A; Pustovarenko A; Hecht S; Gascon J; Kapteijn F; Bleger D Structural Effects in Visible-Light-Responsive Metal-Organic Frameworks Incorporating ortho-Fluoroazobenzenes. Chem. - Eur. J 2016, 22 (2), 746–52. [PubMed: 26617393]

(29). Accardo JV; Kalow JA Reversibly tuning hydrogel stiffness through photocontrolled dynamic covalent crosslinks. Chem. Sci 2018, 9 (27), 5987–5993. [PubMed: 30079213]

(30). Trads JB; Burgstaller J; Laprell L; Konrad DB; de la Osa de la Rosa L; Weaver CD; Baier H; Trauner D; Barber DM. Optical control of GIRK channels using visible light. Org. Biomol. Chem 2016, 15 (1), 76–81. [PubMed: 27901161]

(31). Wegener M; Hansen MJ; Driessen AJM; Szymanski W; Feringa BL Photocontrol of Antibacterial Activity: Shifting from UV to Red Light Activation. J. Am. Chem. Soc 2017, 139 (49), 17979–86. [PubMed: 29136373]

(32). Pfaff P; Samarasinghe KTG; Crews CM; Carreira EM Reversible Spatiotemporal Control of Induced Protein Degradation by Bistable PhotoPROTACs. ACS Cent. Sci 2019, 5 (10), 1682–90. [PubMed: 31660436]

(33). Agnetta L; Bermudez M; Riefolo F; Matera C; Claro E; Messerer R; Littmann T; Wolber G; Holzgrabe U; Decker M Fluorination of Photoswitchable Muscarinic Agonists Tunes Receptor Pharmacology and Photochromic Properties. J. Med. Chem 2019, 62 (6), 3009–3020. [PubMed: 30827105]

(34). Heinrich B; Bouazoune K; Wojcik M; Bakowsky U; Vazquez O ortho-Fluoroazobenzene derivatives as DNA intercalators for photocontrol of DNA and nucleosome binding by visible light. Org. Biomol. Chem 2019, 17 (7), 1827–1833. [PubMed: 30604825]

(35). Lin WC; Tsai MC; Rajappa R; Kramer RH Design of a Highly Bistable Photoswitchable Tethered Ligand for Rapid and Sustained Manipulation of Neurotransmission. J. Am. Chem. Soc 2018, 140 (24), 7445–7448. [PubMed: 29874068]

(36). Saccone M; Siiskonen A; Fernandez-Palacio F; Priimagi A; Terraneo G; Resnati G; Metrangolo P Halogen bonding stabilizes a cis-azobenzene derivative in the solid state: a crystallographic study. Acta Crystallogr., Sect. B: Struct. Sci., Cryst. Eng. Mater 2017, 73 (2), 227–233.

(37). Rastogi SK; Rogers RA; Shi J; Brown CT; Salinas C; Martin KM; Armitage J; Dorsey C; Chun G; Rinaldi P; Brittain WJ Through-space ^{19}F-^{19}F spin-spin coupling in orthofluoro Z-azobenzene. Magn. Reson. Chem 2016, 54 (2), 126–31. [PubMed: 26332615]

(38). Rastogi SK; Rogers RA; Shi J; Gao C; Rinaldi PL; Brittain WJ Conformational Dynamics of o-Fluoro-Substituted ZAzobenzene. J. Org. Chem 2015, 80 (22), 11485–90. [PubMed: 26505924]

(39). Bloembergen N; Purcell EM; Pound RV Nuclear magnetic relaxation. Nature 1947, 160 (4066), 475. [PubMed: 20265559]

(40). Runtsch LS; Barber DM; Mayer P; Groll M; Trauner D; Broichhagen J Azobenzene-based inhibitors of human carbonic anhydrase II. Beilstein J. Org. Chem 2015, 11, 1129–35. [PubMed: 26199669]

(41). Schrödinger Release 2020–1: Maestro; Schrödinger, LLC: New York, NY, 2020.

(42). Kaminski GA; Friesner RA; Tirado-Rives J; Jorgensen WL Evaluation and Reparametrization of the OPLS-AA Force Field for Proteins via Comparison with Accurate Quantum Chemical Calculations on Peptides. J. Phys. Chem. B 2001, 105 (28), 6474– 6487.

(43). Shivakumar D; Williams J; Wu Y; Damm W; Shelley J; Sherman W Prediction of Absolute Solvation Free Energies using Molecular Dynamics Free Energy Perturbation and the OPLS Force Field. J. Chem. Theory Comput 2010, 6 (5), 1509–1519. [PubMed: 26615687]

(44). Khalifah RG The carbon dioxide hydration activity of carbonic anhydrase. I. Stop-flow kinetic studies on the native human isoenzymes B and C. J. Biol. Chem 1971, 246 (8), 2561–2573. [PubMed: 4994926]

(45). Wu Q; Pierce JWM; Delamere NA Cytoplasmic pH Responses to Carbonic Anhydrase Inhibitors in Cultured Rabbit Nonpigmented Ciliary Epithelium. J. Membr. Biol 1998, 162, 31–38. [PubMed: 9516235]

(46). Bonanno JA; Srinivas SP; Brown M Effect of Acetazolamide on Intracellular pH and Bicarbonate Transport in Bovine Corneal Endothelium. Exp. Eye Res 1995, 60, 425–434. [PubMed: 7789422]

(47). Puech C; Chatard M; Felder-Flesch D; Prevot N; Perek N Umbelliferone Decreases Intracellular pH and Sensitizes Melanoma Cell Line A375 to Dacarbazin. Comparison with Acetazolamide. Curr. Mol. Pharmacol 2018, 11 (2), 133–139. [PubMed: 27894244]

(48). Mizumori M; Meyerowitz J; Takeuchi T; Lim S; Lee P; Supuran CT; Guth PH; Engel E; Kaunitz JD; Akiba Y Epithelial carbonic anhydrases facilitate PCO_2 and pH regulation in rat duodenal mucosa. J. Physiol 2006, 573 (Pt 3), 827–842. [PubMed: 16556652]

(49). Rasmussen JK; Boedtkjer E Carbonic anhydrase inhibitors modify intracellular pH transients and contractions of rat middle cerebral arteries during CO_2/HCO3– fluctuations. J. Cereb. Blood Flow Metab 2018, 38 (3), 492–505. [PubMed: 28318362]

(50). Truong L; Harper SL; Tanguay RL Evaluation of embryotoxicity using the zebrafish model. Methods Mol. Biol 2011, 691, 271–79. [PubMed: 20972759]

(51). Postel R; Sonnenberg A Carbonic anhydrase 5 regulates acid-base homeostasis in zebrafish. PLoS One 2012, 7 (6), e39881. [PubMed: 22745834]

(52). Gilmour KM; Perry SF Carbonic anhydrase and acid-base regulation in fish. J. Exp. Biol 2009, 212 (11), 1647–61. [PubMed: 19448075]

(53). Gilmour KM; Thomas K; Esbaugh AJ; Perry SF Carbonic anhydrase expression and CO_2 excretion during early development in zebrafish Danio rerio. J. Exp. Biol 2009, 212 (23), 3837–3845. [PubMed: 19915126]

(54). Matsumoto H; Fujiwara S; Miyagi H; Nakamura N; Shiga Y; Ohta T; Tsuzuki M Carbonic Anhydrase Inhibitors Induce Developmental Toxicity During Zebrafish Embryogenesis, Especially in the Inner Ear. Mar. Biotechnol 2017, 19 (5), 430–440.

(55). Aspatwar A; Becker HM; Parvathaneni NK; Hammaren M; Svorjova A; Barker H; Supuran CT; Dubois L; Lambin P; Parikka M; Parkkila S; Winum JY Nitroimidazole-based inhibitors DTP338 and DTP348 are safe for zebrafish embryos and efficiently inhibit the activity of human CA IX in Xenopus oocytes. J. Enzyme Inhib. Med. Chem 2018, 33 (1), 1064–1073. [PubMed: 29909747]

(56). Westerfield M The zebrafish book: a guide for the laboratory use of zebrafish Danio (Brachydanio) rerio. https://zfin.org/zf_info/zfbook/cont.html (accessed May 20, 2020).

(57). Kimmel CB; Ballard WW; Kimmel SR; Ullmann B; Schilling TF Stages of embryonic development of the zebrafish. Dev. Dyn 1995, 203 (3), 253–310. [PubMed: 8589427]
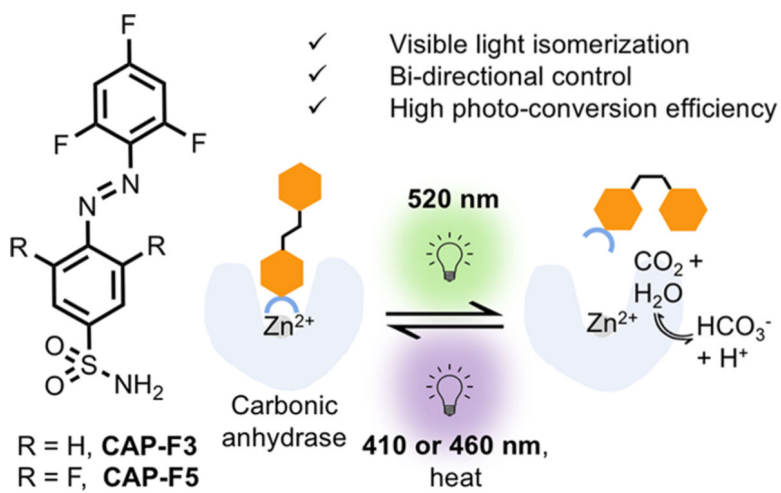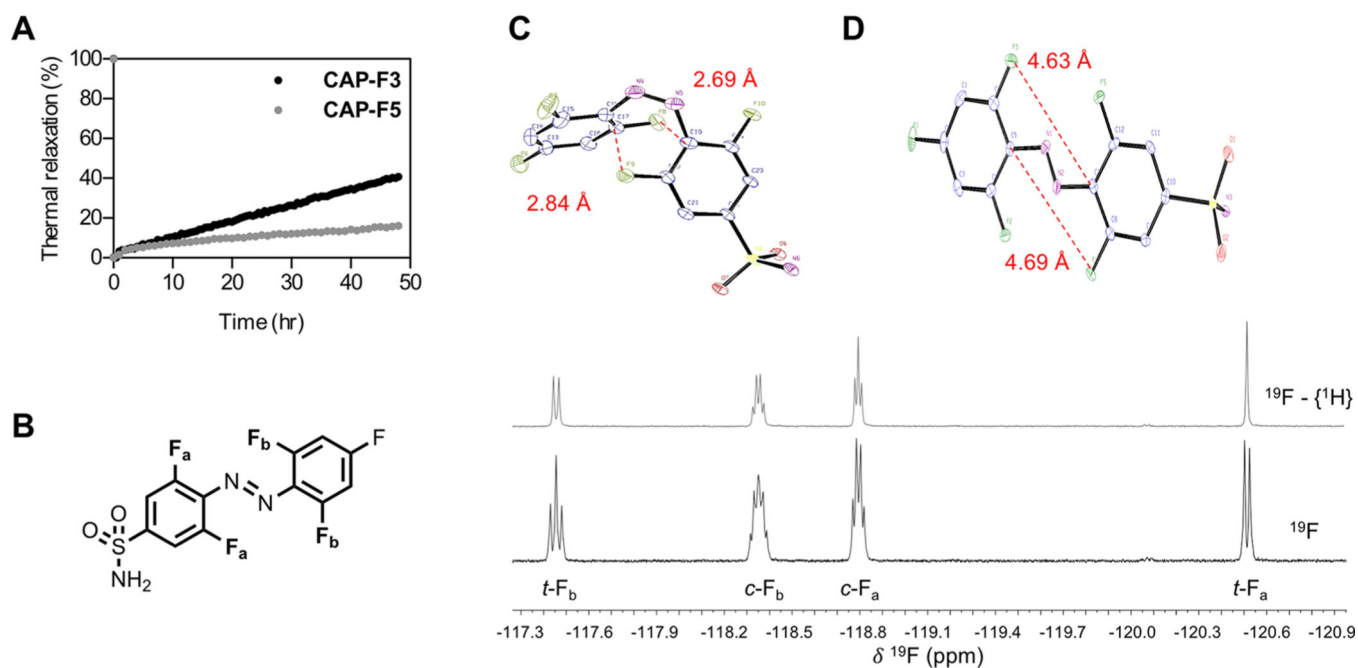
**Scheme 1. Structures of CAP-F3 and CAP-F5 and Photoswitching in the Presence of Carbonic Anhydrase**
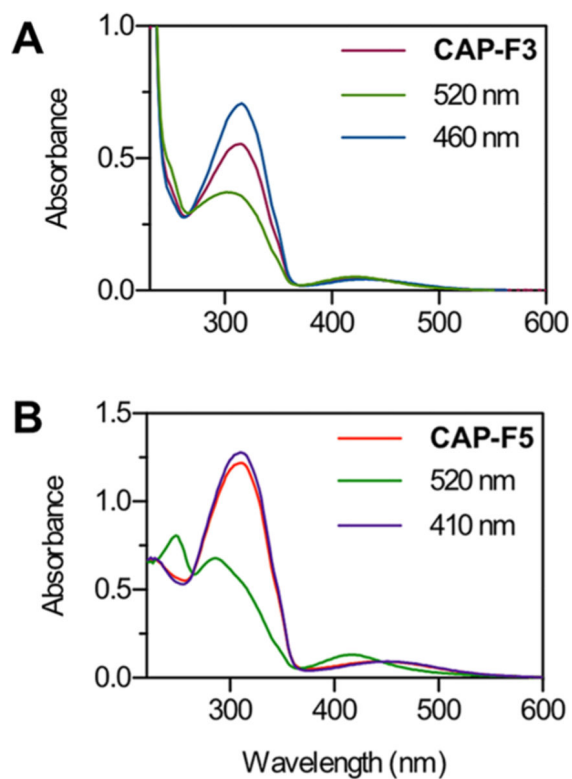
Figure 1.
UV-vis spectra of CAP-F3 (A) and CAP-F5 (B) before and after photoirradiation (*cis* 520 nm for 5 min; *trans* 460/410 nm for 2 min). The power densities for 410, 460, and 520 nm were 5.20, 14.12, and 9.18 mW/cm^2, respectively. The studies are performed in methanol at 298 K.
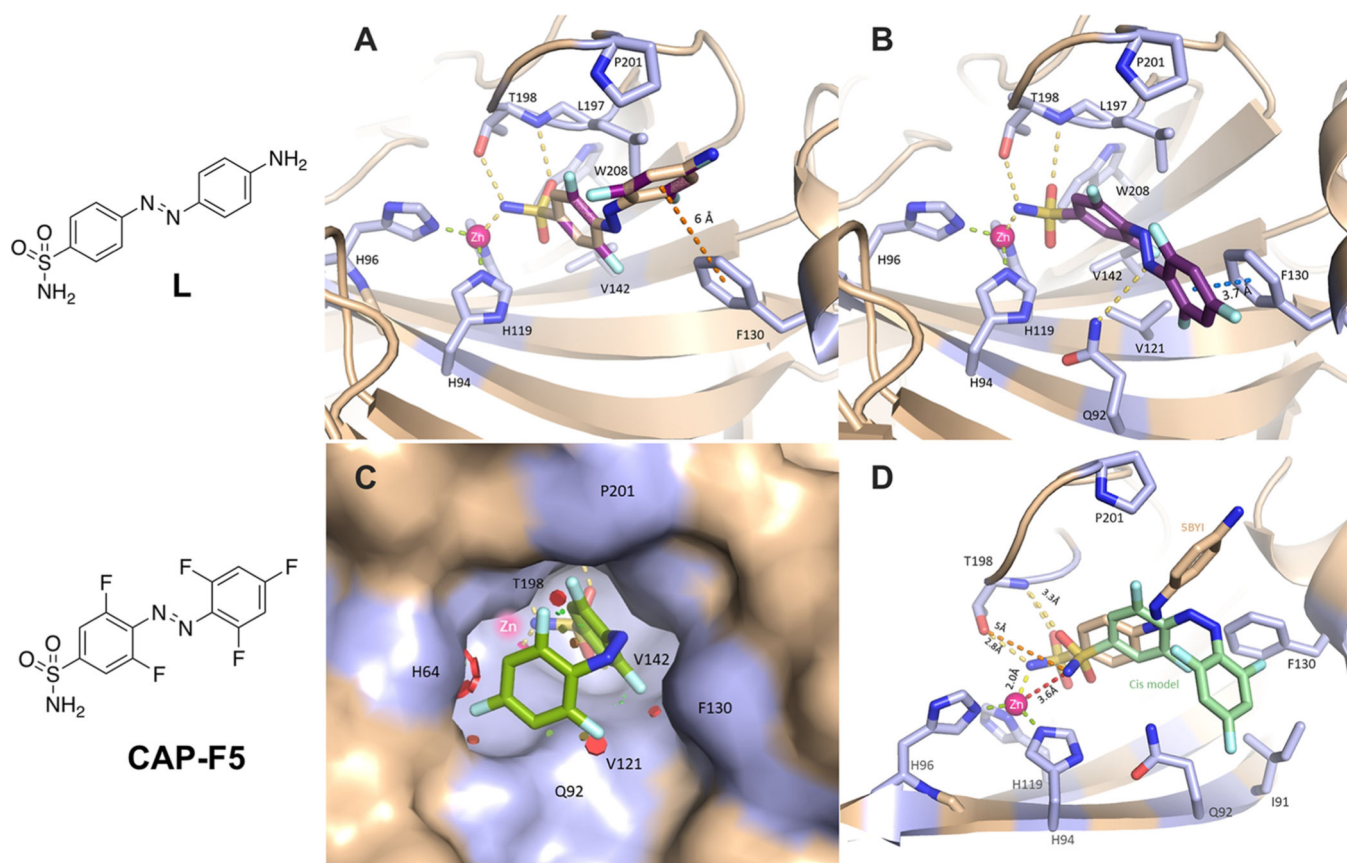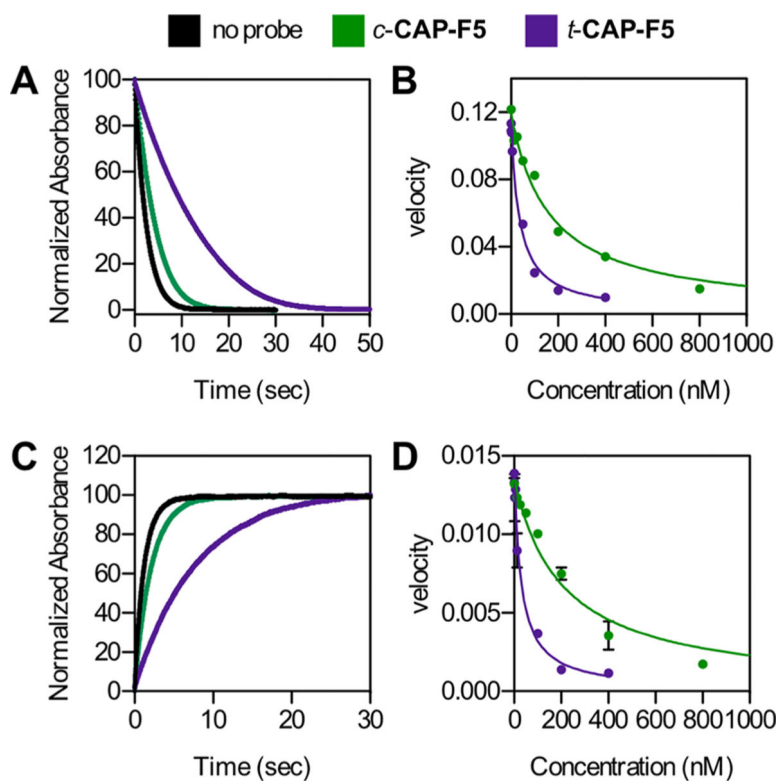
Figure 2.
(A) Thermal relaxation of *c*-CAP-F3 and *c*-CAP-F5 in aqueous buffer at 37 °C. (B) ^{19}F and ^{19}F-{^{1}H} NMR spectra for CAP-F5 collected in CD$_3$OD. Single crystal structure of *c*-CAP-F5 (C) and *t*-CAP-F5 (D). Thermal ellipsoid plots at 50% probability are shown. Solvent molecules and hydrogen atoms are omitted for clarity.
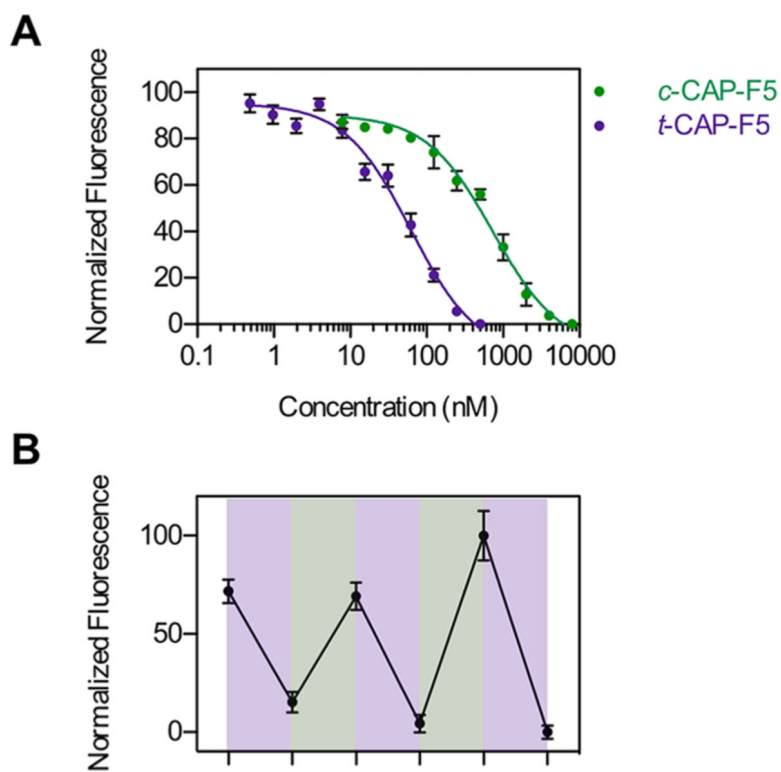
Figure 3.
(A) Change in fluorescence emission (λ_{ex} = 280 nm; λ_{em} = 458 nm) of bCA-DNSA mixture in the presence of different concentrations of *t*-CAP-F5 and *c*-CAP-F5 to determine apparent K_d values. (B) The binding of CAP-F5 is reversible in nature, as shown by irradiating the samples of CA, DNSA, and probe with alternate 520 and 410 nm for *in situ* isomerization and monitoring DNSA fluorescence. Data represent mean ± standard deviation. Studies conducted in 50 mM HEPES, 0.1 M KNO_3, pH 7.2, 298 K, in the dark.
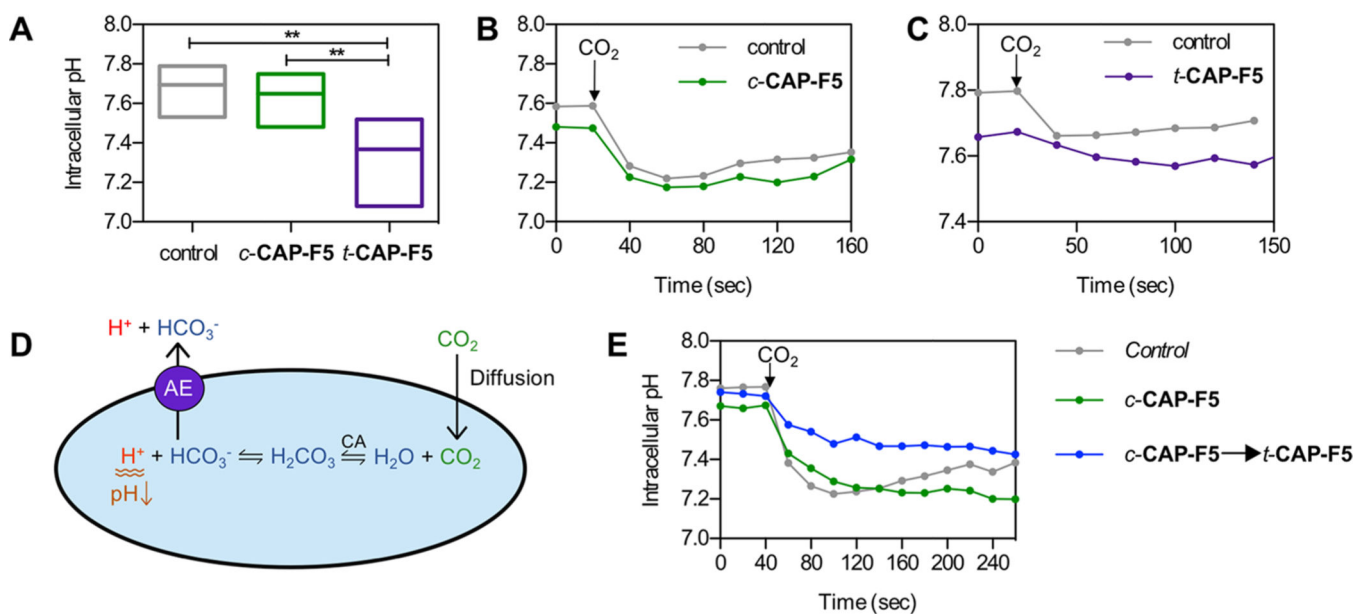
Figure 4.
Docking of CAP-F5 in the active site of hCAII structure obtained with azobenzene ligand L
bound to the active site (PDB 5BYI). The secondary protein (PDB 5BYI) is shown with side
chains of active site residues in sticks. The favorable hydrogen bonds and $\pi-\pi^*$ interactions
are shown in yellow and orange dotted lines, respectively. (A) Docking of t-CAP-F5 into the
hCAII active site after superimposing it onto the ligand L. (B) Alternative binding mode for
t-CAP-F5 due to the presence of fluorine atoms. (C) Docking of c-CAP-F5 when
interactions between $-SO_2NH_2$ and Zn^{2+} are kept intact, steric clashes are shown as red
disks. (D). Potential orientation of c-CAP-F5 when steric clashes are removed, showing the
probe retreats from the active site.

Figure 5.

Change in absorbance of phenol red (λ = 557 nm) due to CO_2 hydration activity (A) and HCO_3^- dehydration activity (C) of CA in the absence and presence of 1 equiv of *trans* and *cis* CAP-F5. Change in CO_2 hydration (B) and HCO_3^- dehydration (D) catalytic velocity (s^{-1}) as a function of *trans* and *cis* isomer concentration. Studies are conducted in 50 mM HEPES, 0.1 M KNO_3 pH 7.2 at 25 °C using stop flow apparatus. Data represent mean $\pm$ the standard deviation.

Figure 6.
(A) The intracellular pH of HeLa cells as a result of incubation of *t*-CAP-F5 and *c*-CAP-F5 for 30 min, as analyzed by flow cytometry. The results are shown as an average of six independent experiments. Box plot indicates the range and average values for each group. Asterisks denote statistically significant differences ($p < 0.05$; one-way analysis of variance). The change in intracellular pH with respect to time as a result of addition of CO_2 in the presence of *c*-CAP-F5 (B) and *t*-CAP-F5 (C) due to the mechanism shown in (D). (E) The change in intracellular pH of cells incubated with *c*-CAP-F5 before and after irradiating with 410 nm to isomerize *cis* isomer to *trans* isomer in situ. These studies were performed in Live Cell Imaging Solution at 4 °C.
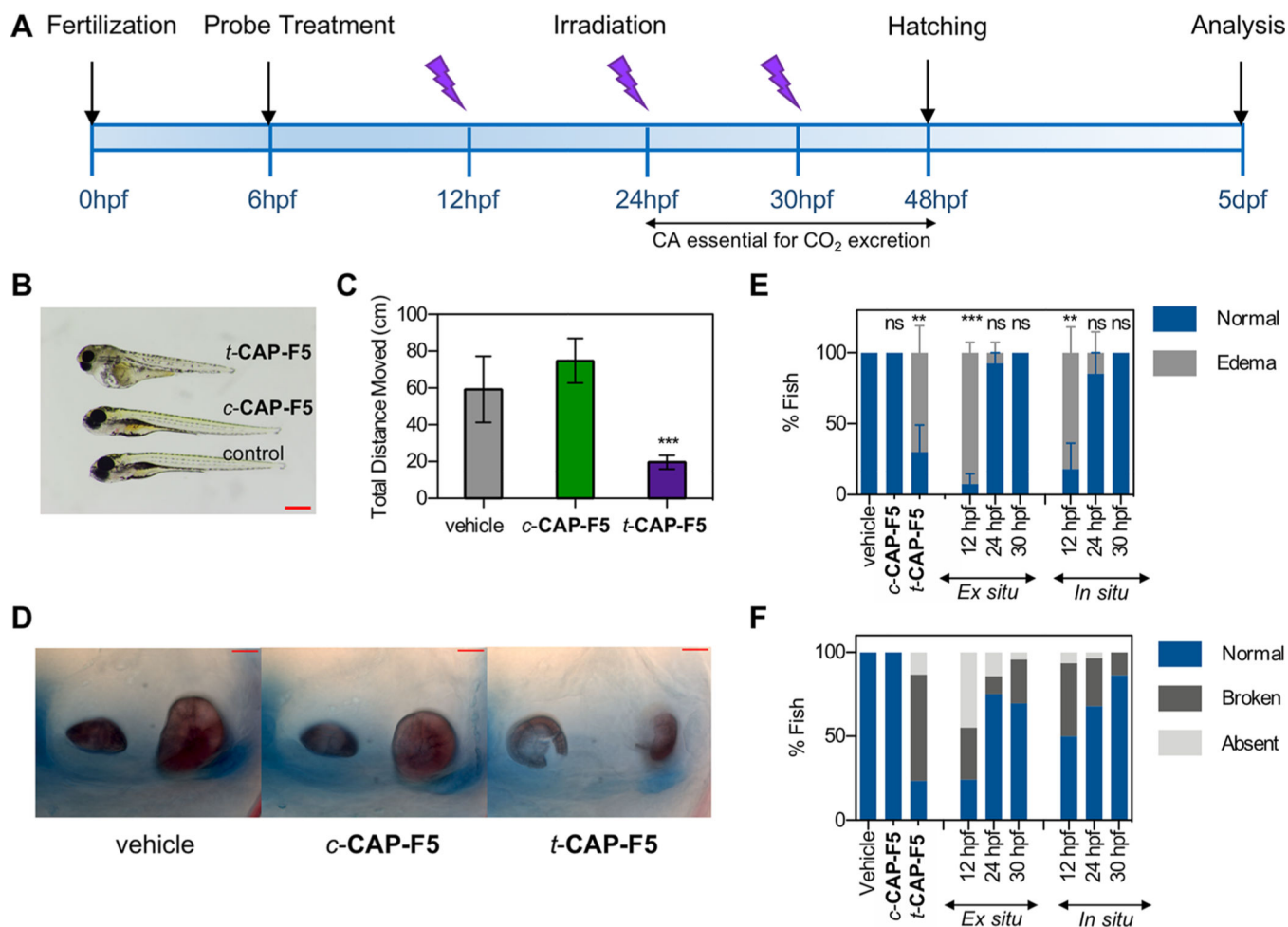
Figure 7.
(A) The timeline representing probe treatment and fish analysis. The morphological appearance (B), swimming behavior (C), and otolith development (D) in fish in the absence (vehicle) and presence of *t*-CAP-F5 and *c*-CAP-F5. The data represents mean values ± the standard deviation. Asterisks denote statistically significant differences ($p < 0.0001$; one-way analysis of variance). Scale bars represent 500 and 50 μm for B and D, respectively. The morphological (E) and otolith (F) development as a result of *in situ* activation of probe from *cis* to *trans* isomer by irradiating the fish with 410 nm at different time points during embryo development. These developments are compared with *ex situ* generated *trans* isomer treatment at the respective time points. The representative images for normal, broken, and absent otoliths can be found in the Supporting Information. The results are represented as mean of 30 fish in 3 independent experiments. Data represent mean values ± SEM. Asterisks denote statistically significant differences (**$p < 0.005$, ***$p < 0.0001$; one-way analysis of variance).